Support Vector Analysis of Color-Doppler Images: A New Approach for Estimating Indices of Left Ventricular Function

J. L. Rojo-Álvarez, *Member, IEEE*, J. Bermejo*, V. M. Juárez-Caballero, R. Yotti, C. Cortina, M. A. García-Fernández, and J. C. Antoranz

***Abstract*—Reliable noninvasive estimators of global left ventricular (LV) chamber function remain unavailable. We have previously demonstrated a potential relationship between color-Doppler M-mode (CDMM) images and two basic indices of LV function: peak-systolic elastance ($E_{\max}$) and the time-constant of LV relaxation (τ). Thus, we hypothesized that these two indices could be estimated noninvasively by adequate postprocessing of CDMM recordings. A semiparametric regression (SR) version of support vector machine (SVM) is here proposed for building a blind model, capable of analyzing CDMM images automatically, as well as complementary clinical information. Simultaneous invasive and Doppler tracings were obtained in nine mini-pigs in a high-fidelity experimental setup. The model was developed using a test and validation leave-one-out design. Reasonably acceptable prediction accuracy was obtained for both $E_{\max}$ (intraclass correlation coefficient $R_{ic} = 0.81$) and τ ($R_{ic} = 0.61$). For the first time, a quantitative, noninvasive estimation of cardiovascular indices is addressed by processing Doppler-echocardiography recordings using a learning-from-samples method.**

***Index Terms*—Doppler-echocardiography, elastance, left ventricular function, noninvasive, semiparametric regression, support vector machine, time-constant of relaxation.**

I. Introduction

A FULL noninvasive characterization of left ventricular (LV) function in the clinical setting is still a pending issue. At a chamber integration level, vast theoretical and experimental research has established the time-constant of relaxation (τ) and the peak systolic elastance ($E_{\max}$) as the best available indicators of LV relaxation, and global systolic chamber function, respectively (see [1]–[3] for recent reviews). However, a direct measurement of these indices is not possible for standard patient management because they require sophisticated, expensive, and potentially hazardous, catheterization procedures.

Because it is fully noninvasive, portable, and inexpensive, Doppler-echocardiography is the most generalized technique to assess cardiovascular function in patients. However, most aspects of LV physiology are approximated indirectly using this technique. Estimating the status of LV diastolic function from the analysis of pulsed-wave Doppler spectrograms is a typical example of such approach [2], [4]. Although this Doppler-echocardiography assessment of diastolic function allows investigators to separate different disease groups, its accuracy is limited to establish diagnosis and guide therapy in a particular patient [5], [6].

Research in the field of noninvasive characterization of LV function has usually followed a typical pattern of development. First, a theoretical model is proposed based on the physical laws of fluid-dynamics that relate invasive and noninvasive measurements. Then, this prespecified relationship is calibrated and tested using animal or clinical experiments, most frequently using simple univariant regression. The accuracy and reliability of the method is then assessed in a different population by the same or other investigators. Finally, the definitive application of the method in clinical practice generally requires incorporating complementary clinical information to obtain the highest efficiency for medical decision making. An example of this typical pattern of research in the field of diastolic function can be followed in [7] (relationship definition and preliminary testing), [8], [9] (assessment of reliability), and [10] (incorporation of clinical information).

The present study proposes a different approach. A physically-determined relationship is also assumed to exist between fundamental hemodynamic variables (flow-rate, pressure, and volume) and the physiological properties of the heart. However, we do not prespecify the basis of such a relationship; instead, we propose a learning from samples algorithm applied to a large data set. For this purpose, an accurate measurement of the distribution of at least one low-level hemodynamic variable is required, assuming that the other variables can be obtained by a nonlinear (yet unknown) transformation of the chosen magnitude.

Although constrained to one spatial dimension, color-Doppler M-mode (CDMM) echocardiography provides a very accurate spatiotemporal distribution of flow velocity within the heart. Furthermore, by means of Euler's momentum equation, we have already demonstrated that there is a physiological

Manuscript received October 11, 2005; revised March 22, 2006. This work was supported in part by the Fondo de Investigación Sanitaria under Research Grant PI031220 of the Instituto Carlos III, Madrid, Spain, and in part by a research grant from the Sociedad Española de Cardiología, 2003. The work of R. Yotti was supported by the Instituto Carlos III under Grant BEFI BF03-00031. *Asterisk indicates corresponding author.*

J. L. Rojo-Álvarez and V. M. Juárez-Caballero are with the Department of Signal Theory and Communications, Universidad Carlos III de Madrid, 28911 Madrid, Spain .

*J. Bermejo is with the Department of Cardiology, Hospital General Universitario Gregorio Marañón, 28007 Madrid, Spain (e-mail: javbermejo@jet.es).

R. Yotti, C. Cortina, and M. A. García-Fernández are with the Department of Cardiology, Hospital General Universitario Gregorio Marañón, 28007 Madrid, Spain.

J. C. Antoranz is with Department of Mathematical Physics and Fluids, Universidad Nacional de Educación a Distancia, 28040 Madrid, Spain.

Digital Object Identifier 10.1109/TMI.2006.875437

basis that relates ejection velocities to τ and $E_{\max}$ [11]–[13]. Attempting to estimate a diastolic index as τ from purely systolic velocity data may seem adventurous. However, previous wave intensity analysis experiments have demonstrated a physiological relationship between τ and end-ejection flow events [14]. Thus, we hypothesized that τ and $E_{\max}$ could be predicted from CDMM-images of LV ejection flow.

A learning from examples procedure can be suitable for assessing this relationship at a reasonable computational cost. Neural networks have been used previously in clinical echocardiography for automated image feature extraction, and for automatic diagnosis of heart disease [15]–[19]. However, all these methods have focused on a classification framework, which represents a softer problem than estimating a continuous index. Furthermore, some kind of image feature extraction algorithm always needs to be performed before classification, as full image consideration is precluded due to its high dimensionality. To our knowledge, learning from samples techniques have never been used for estimating directly a quantitative index of cardiovascular function from a medical image. In this paper, we propose the use support vector machines (SVM) for this purpose.

The outline of the paper is as follows. First, the SVM semiparametric regression is justified, described, and expressed in terms of our problem. Then, the type of images and hemodynamic measurements performed are introduced. After method description, experiments with CDMM images in an animal model explore the feasibility of the noninvasive learning from images method for estimating the two proposed cardiac indices. Conclusions are finally drawn.

II. Formulation

SVM have emerged recently in the field of learning from samples applications due to a number of well-proven properties [20]. SVM work well for high-dimensional input spaces (as those given by images or gene expression); they have a single minimum; large scale algorithms are continuously being developed; and they exhibit excellent generalization performance. We propose to use a semiparametric regression (SR) version of SVM (SVM-SR) [21], which will allow us both to efficiently combine nonlinearity (Gaussian kernel for image analysis) with parametric inclusion of information (linear kernel for clinical variables). Due to our incomplete knowledge about the underlying noise distribution, the ε-Huber cost is considered here, as described in [22], for a robust estimation approach.

We propose [21] to explore the possibility of modeling the functional relationship between the spatiotemporal velocity field, as recorded noninvasively in the CDMM image, and the value of a simultaneously invasively measured hemodynamical index y. The use of SVM allows us to include, if necessary, additional noninvasive clinical variables in the model. Let $\mathbf{x}^v$ denote a V-dimensional vector containing a CDMM image, and $\mathbf{x}^c$ a C-dimensional vector with clinical measurements. Assume that there exists a possibly nonlinear transformation of the velocity vector (clinical features vector) into a higher dimensionality space, $\varphi(\mathbf{x}^v) : \mathbb{R}^V \rightarrow \mathfrak{F}_v(\phi(\mathbf{x}^c) : \mathbb{R}^C \rightarrow \mathfrak{F}_c)$, where $\mathfrak{F}_v(\mathfrak{F}_c)$ is known as *feature space*. A linear regression operator can be found in each feature space for each set of input variables, given by $\mathbf{w} \in \mathfrak{F}_v(\mathbf{v} \in \mathfrak{F}_c)$. Assume that a set of measured observations $\{y_i, \mathbf{x}_i^v, \mathbf{x}_i^c\}$, with $i = 1, \ldots, N$, is available. Under these assumptions, the combined regression model is

$$y_i = \langle \mathbf{w}, \varphi(\mathbf{x}_i^v) \rangle + \langle \mathbf{v}, \phi(\mathbf{x}_i^c) \rangle + b_r + e_i \tag{1}$$

where b_r is the intercept, and e_i represent the model errors or residuals.

The SVM methodology [20] allows us to use different cost functions of the residuals. A suitable robust cost function, that has been proposed for time series and regression-like problems, is the ε-*Huber cost*, given by

$$L^P(e_i) = \begin{cases} 0, & |e_i| \leq \varepsilon \\ \frac{1}{2\gamma}(|e_i| - \varepsilon)^2, & \varepsilon \leq |e_i| \leq e_C \\ C(|e_i| - \varepsilon) - \frac{1}{2}\gamma C^2, & |e_i| \geq e_C \end{cases} \tag{2}$$

where $e_c = \varepsilon + \gamma C$. This cost function has been shown to be useful in the presence of non-Gaussian perturbations, and can be adapted to different kinds of noise [22], [23]. The algorithm, described in [21], consists of minimizing the ε-Huber cost when it is regularized with the L_2 norm of both regression vectors, this is, we minimize

$$L_P(\mathbf{w}, \mathbf{v}, \xi_i, \xi_i^*, b_r) = \frac{1}{2}\left(\|\mathbf{w}\|^2 + \|\mathbf{v}\|^2\right) + \frac{1}{2\gamma}\sum_{i \in I_1}\left(\xi_i^2 + \xi_i^{*2}\right) + C\sum_{i \in I_2}(\xi_i + \xi_i^*) - \sum_{i \in I_2}\frac{\gamma C^2}{2} \tag{3}$$

constrained to

$$y_i - \langle \mathbf{w}, \varphi(\mathbf{x}_i^v) \rangle - \langle \mathbf{v}, \phi(\mathbf{x}_i^c) \rangle - b_r \leq \varepsilon + \xi_i \tag{4}$$

$$-y_i + \langle \mathbf{w}, \varphi(\mathbf{x}_i^v) \rangle + \langle \mathbf{v}, \phi(\mathbf{x}_i^c) \rangle + b_r \leq \varepsilon + \xi_i^* \tag{5}$$

and to $\xi_i, \xi_i^* \geq 0$, where ξ_i and ξ_i^* (in the following, denoted jointly as $\xi_i^{(*)}$) are the slack variables that account for the excess of the residuals over insensitivity ε, and $I_1(I_2)$ is the set of samples for which $\varepsilon \leq \xi_i^{(*)} \leq e_C(\xi_i^{(*)} > e_C)$. By following the usual SVM formulation methodology, Lagrangian functional L_{PD} can be written [20], [22], and by making zero its gradient with respect to the primal variables, we obtain

$$\nabla_{\mathbf{w}} L_{PD} = 0 \Rightarrow \mathbf{w} = \sum_{i=1}^{N}(\alpha_i - \alpha_i^*)\varphi(\mathbf{x}_i^v) \tag{6}$$

$$\nabla_{\mathbf{v}} L_{PD} = 0 \Rightarrow \mathbf{v} = \sum_{i=1}^{N}(\alpha_i - \alpha_i^*)\phi(\mathbf{x}_i^c) \tag{7}$$

$$\nabla_{\xi^{(*)}} L_{PD} = 0 \Rightarrow 0 \leq \alpha_i^{(*)} \leq C \tag{8}$$

$$\nabla_{b_r} L_{PD} = 0 \Rightarrow \sum_{i=1}^{N}(\alpha_i - \alpha_i^*) = 0 \tag{9}$$

where α_i, α_i^* denote the Lagrange multipliers that correspond to (4), (5), respectively. Matrix notation is introduced as follows:

$$\mathbf{y} = [y_1, \ldots, y_N]^T \tag{10}$$

$$\boldsymbol{\alpha}^{(*)} = \left[\alpha_1^{(*)}, \ldots, \alpha_N^{(*)}\right]^T \tag{11}$$

$$\mathbf{V}(i,j) = \left\langle \varphi(\mathbf{x}_i^v), \varphi\left(\mathbf{x}_j^v\right) \right\rangle \tag{12}$$

$$\mathbf{C}(i,j) = \left\langle \phi\left(\mathbf{x}_i^c\right), \phi\left(\mathbf{x}_j^c\right) \right\rangle \tag{13}$$

and then, the dual problem consists of maximizing

$$L_D(\boldsymbol{\alpha}, \boldsymbol{\alpha}^*) = -\frac{1}{2}(\boldsymbol{\alpha} - \boldsymbol{\alpha}^*)^T(\mathbf{V} + \mathbf{C} + \gamma\mathbf{I})(\boldsymbol{\alpha} - \boldsymbol{\alpha}^*) + (\boldsymbol{\alpha} - \boldsymbol{\alpha}^*)^T\mathbf{y} - \varepsilon(\boldsymbol{\alpha} + \boldsymbol{\alpha}^*)^T\mathbf{1} \tag{14}$$

with respect to $\alpha_i^{(*)}$, and constrained to (8) and (9). After this quadratic programming (QP) problem is solved, and according to (1), (6), and (7), the estimated output $\hat{y}$ for a new observation $\mathbf{x}$ can be easily shown to be given by

$$\hat{y} = \sum_{i=1}^{N} \eta_i \left(\left\langle \varphi\left(\mathbf{x}_i^v\right), \varphi(\mathbf{x}^v) \right\rangle + \left\langle \phi\left(\mathbf{x}_i^c\right), \phi(\mathbf{x}^c) \right\rangle \right) + b_r \tag{15}$$

where $\eta_i = (\alpha_i - \alpha_i^*)$. This solution has a sparse expression for an adequate choice of $\varepsilon > 0$, as it only depends of the observations with $\eta_i \neq 0$. These observations with non-null coefficient are called support vectors, and they contain all the information that is necessary for the model.

Additionally, the SVM methodology takes profit of Mercer's kernels to avoid the calculation of dot products in feature spaces in (15). A Mercer's kernel is a bivariate function $K()$ that is equivalent to calculating a dot product in a possibly infinite dimensional feature space [24], this is, a Mercer's kernel fulfills $K(\mathbf{x}, \mathbf{y}) = \langle \varphi(\mathbf{x}), \varphi(\mathbf{y}) \rangle$. Hence, if we use valid Mercer's kernels, we do not need even to explicitly consider the nonlinear transformation. Examples of valid and widely used Mercer's kernels are the following.

- The *linear kernel*, given by $K_p(\mathbf{x}, \mathbf{y}) = \langle \mathbf{x}, \mathbf{y} \rangle$. In this case, the regression function has a linear form that can be calculated explicitly as

$$\boldsymbol{\beta} = \sum_{i=1}^{N} \eta_i \mathbf{x}_i^c. \tag{16}$$

- The *Gaussian kernel*, given by

$$K_{np}(\mathbf{x}, \mathbf{y}) = \exp\left(-\frac{\|\mathbf{x} - \mathbf{y}\|^2}{2\sigma^2} \right) \tag{17}$$

  where σ is the width parameter. From a computational point of view, (14) is a well-defined QP problem (it has a single minimum) for any nondegenerate value of this free parameter.

Therefore, we can use in our model a composite Mercer's kernel, obtained as the sum of a (scaled) linear kernel that accounts for the parametric component

$$\left\langle \phi\left(\mathbf{x}_i^c\right), \phi\left(\mathbf{x}_j^c\right) \right\rangle = K_p\left(\mathbf{x}_i^c, \mathbf{x}_j^c\right) = \delta \left\langle \mathbf{x}_i^c, \mathbf{x}_j^c \right\rangle \tag{18}$$

plus a nonlinear kernel that generates the nonparametric component

$$\left\langle \varphi\left(\mathbf{x}_i^v\right), \varphi\left(\mathbf{x}_j^v\right) \right\rangle = K_{np}\left(\mathbf{x}_i^v, \mathbf{x}_j^v\right). \tag{19}$$

Constant $\delta > 0$ can be chosen for giving an adequate balance between the parametric and the nonparametric components. Thus, the final solution in (15) can be readily expressed as

$$\hat{y} = \sum_{i=1}^{N} \eta_i K_{nl}\left(\mathbf{x}_i^v, \mathbf{x}^v\right) + \delta \langle \boldsymbol{\beta}, \mathbf{x}^c \rangle + b_r. \tag{20}$$

Taking (16) and (20) into account, we see that coefficients η_i determine completely both the parametric and the nonparametric components of the model.

In general, two kinds of free parameters must be chosen: cost function free parameters $\{\gamma, C, \varepsilon\}$, and kernel free parameters $\{\sigma, \delta\}$. A possible method for setting them is a sequential search of the appropriate value for each, based on bootstrap bias-corrected training error, as proposed in [25], and this is the approach followed in this paper.

III. Experiments and Results

A. Data Acquisition

$E_{\max}$ and τ were chosen as the indices to be predicted because they are currently accepted as the best available standards of two crucial properties of the LV. τ accounts for the time-constant of LV pressure decay, and measures the rate of LV relaxation during the isovolumic phase. $E_{\max}$ accounts for peak end-systolic LV elastance, and it is the best index to assess global LV systolic chamber function. The methodological details of the animal experiments used for the present study have been reported elsewhere [12]. Briefly, using an open-chest animal setup, simultaneous EKG, high-fidelity pressure (solid-state micromanometers), volume (conductance catheter), and CDMM recordings were obtained in nine mini-pigs under variable hemodynamic conditions induced by pharmacological interventions and acute ischemic cardiomyopathy. After recording baseline values, acquisition of invasive pressure and volume data was continued during preload reduction by occlusion of the inferior vena cava. Invasive signals were digitized at 1000 Hz and CDMM images were stored in DICOM III format for offline processing. Analysis of the same beat of CDMM and invasive recordings was ensured by retrospective cross-correlation matching of a synchronicity signal [11], [12]. τ was calculated from the high-fidelity pressure signal using the zero-asymptote assumption [26] by nonlinear regression fitting. The iterative linear regression method was used to calculate $E_{\max}$ [27]. Consequently, for each CDMM recording matched values of τ (same beat) and $E_{\max}$ (immediately following beats during cava occlusion) were obtained.

CDMM images were obtained using a phase-array broadband 2.0–4.0-MHz transducer on a Sequoia C-256 system (Siemens AG), from an epicardial approach [12]. These CDMM tracings display the 1-dimensional spatiotemporal map of ejection flow velocity along the long axis of the LV. Velocity values were obtained from the color values of each pixel using a previously validated decoding and de-aliasing algorithm [28]. Spatial and temporal calibration was obtained automatically from the DICOM metadata; velocity calibration was obtained by automatic reading of the images scale limits. The beginning and

TABLE I
NUMBER OF TRAINING AND TEST OBSERVATIONS FOR EACH REGRESSION MODEL

Reg.	#1	#2	#3	#4	#5	#6	#7	#8	#9
Train	247	253	276	255	251	234	243	236	253
Test	34	28	5	26	30	47	38	45	28

end of ejection, as well as the positions of the LV apex and outflow tract, were visually identified in each image. CDMM recordings were then aligned and cropped slightly beyond these limits, interpolated using a bivariate tensor product spline, and then downsampled to a grid of $2^d \times 2^d$ pixels, where d is a free parameter of the preprocessing that will be called detail in the successive. For the $E_{\max}$ estimations, downsampled CDMM images were the input to the SVM, and no parametric component was considered ($\delta = 0$). Based on previous studies from our group [12], we assumed that it should be possible to predict $E_{\max}$ with reasonable accuracy using only the CDMM as the input space of the SVM. For the τ estimations, we also explored the advantage of incorporating the following variables into the parametric component of the model: heart-rate (HR), peak LV pressure (LVP), LV ejection fraction (EF, obtained automatically from the conductance signal), and their squared values. Importantly, in clinical practice these additional variables can be readily obtained noninvasively by sphygmomanometry and B-mode cross-sectional echocardiography.

B. Data Analysis

Given that intra-subject measurements are expected to be strongly dependent, we considered the following development strategy. All the available measurements in all but one animal were considered for training, and the measurements for the left-out animal were used as the independent test set; this procedure was repeated for the nine available pigs. Table I shows the resulting number of observations in each train and test set for each of the nine leave-one-animal-out regression model.

For the image-based components of the input spaces, not only the RBF kernel, but also the linear kernel, were explored. For each regression model, the required free parameters were adjusted in the training set. Searched free parameters were 1) cost function parameters $\{\gamma, C, \varepsilon\}$, in all the cases and 2) kernel parameters $\{\sigma, \delta\}$ as required by each input feature space. Free parameters were adjusted for providing the minimum bootstrap mean squared error, by following a procedure similar to that proposed in [25], and using $B = 10$ bootstrap resamples. In order to assess the agreement between measured and predicted measurements of $E_{\max}$ and τ, the intraclass correlation coefficient (R_{ic}) was used as merit figure for each regression model calculated.

For the first set of experiments, a value of $d = 4$ was fixed, so that the downsampled images were 16×16 pixels. This value of d was an initial tradeoff between a moderate computational burden and a minimally acceptable representation of the velocity field in the image.

C. Prediction Accuracy

Table II shows the R_{ic} values when estimating $E_{\max}$ for each regression model, as well as for the whole set of the independent outputs. The highest performance ($R_{ic} = 0.81$) was achieved by the linear kernel, and surprisingly, the RBF kernel was not able to improve this approximation performance. Fig. 1(a) and (b) depicts the predicted $E_{\max}$ for each observation, as provided by its own independently trained machine. Though the accuracy in the prediction was limited, a good trend to follow the actual output value was observed. The Bland–Altman plot demonstrates a nonuniform distribution of error and greatest imprecision is observed for the highest values of $E_{\max}$ obtained during inotropic stimulation. Fortunately, accuracy in this range is less relevant than at the low contractility level, and a certain amount of uncertainty at supraphysiological values is unlikely to have any impact on clinical decision making.

TABLE II
VALUES OF R_{ic} FOR EACH SVR ESTIMATING $E_{\max}$, FROM VELOCITY (V), WITH $d = 4$ (LINEAR AND GAUSSIAN KERNEL)

	V lin	V Gauss
#1	0.37	0.67
#2	0.58	0.41
#3	0.54	0.16
#4	0.61	0.36
#5	0.83	0.72
#6	0.30	0.53
#7	0.75	0.45
#8	0.55	0.34
#9	0.76	0.32
Total	0.81	0.67

Table III shows the R_{ic} values when estimating τ. In this case, the highest performance was given by the combined input space using a linear kernel ($R_{ic} = 0.61$), though there was no significant difference with respect to the velocity-only input space. Fig. 1(c) and (d) shows predicted τ following the invasive gold-standard value, but with a relative uncertainty greater than for $E_{\max}$ prediction case. Again, the use of RBF kernel for the image input space did not improve the estimation, but, instead, showed lower values of total R_{ic} (not shown).

The advantages of including clinical features in the input space for predicting τ is shown in Table III, and the value and 95% confidence intervals of the parametric components (for $d = 4$) are shown in Table IV. Although a number of these coefficients were significant, the increase in model accuracy was small in most experiments. In all cases, parameter δ in (20) was optimized, to compensate for possible differences in the relative relevance of the CDMM image and the clinical features input variables.

To assess the relative weight of each region in the CDMM image to predict τ and $E_{\max}$, the coefficients resulting from the regressions were analyzed. For this purpose, standardized regression coefficients corresponding to image pixels in the input space for each of the nine experiments were calculated, as well as their spatial average (Fig. 2). Notice that most relevant information in the CDMM image for estimating $E_{\max}$ was found during the onset of the ejection flow velocity field, at approximately 10% of ejection time, and that higher velocities were related to higher values of $E_{\max}$ (positive mean standardized coefficients). This observation is in close accordance with our previous finding relating $E_{\max}$ to the peak-ejection intraventricular pressure gradient caused by early systolic local flow acceleration [12]. Similarly, most relevant information in the

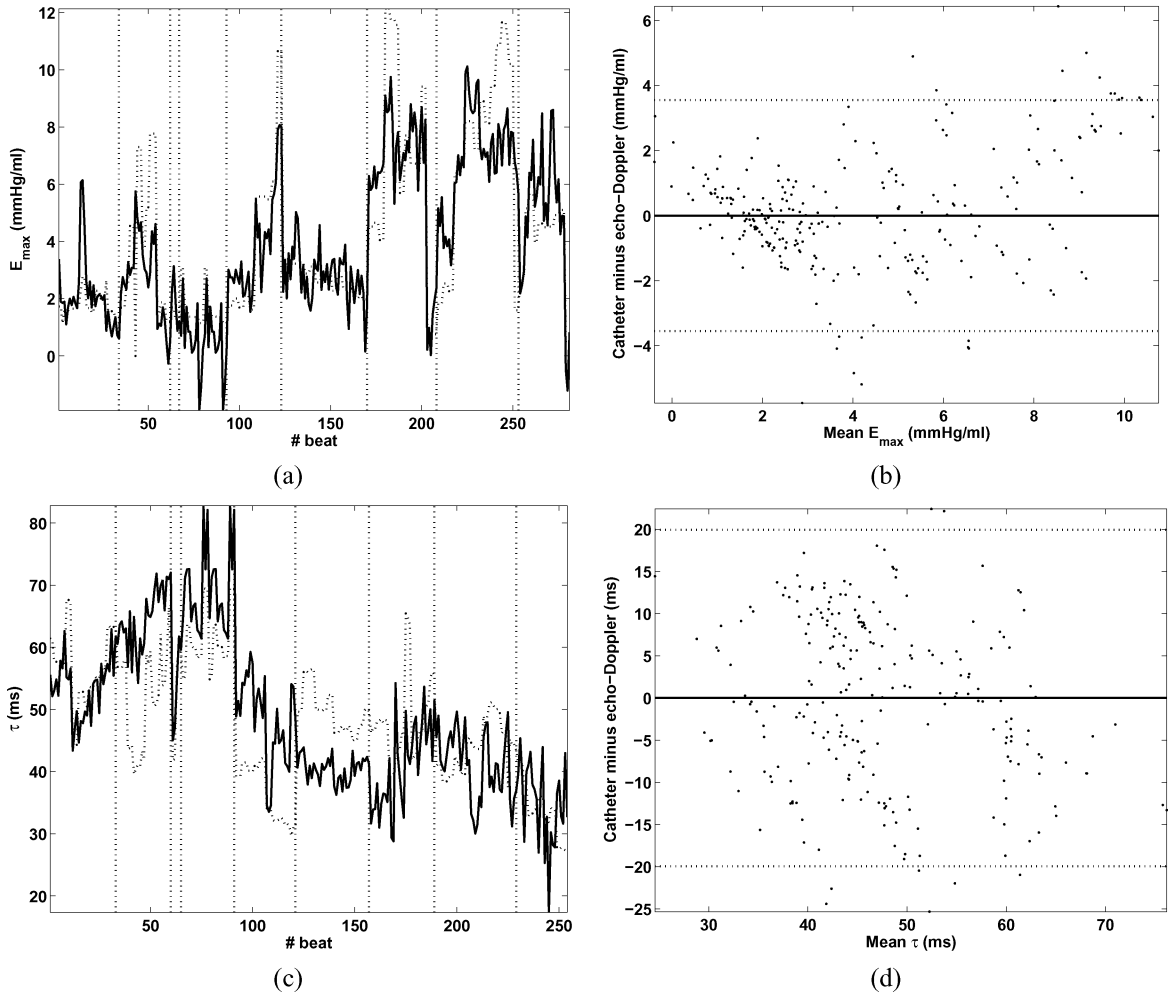

Fig. 1. Predicted values of $E_{\max}$ with $d = 4$ and linear kernel. (a) Noninvasive prediction for each observation (continuous) and catheter measurement (dashed), vertical lines separate observations from different animals. (b) Bland–Altman plot of errors (dotted line represents two standard deviations). Predicted values of τ with $d = 4$, velocity and clinical features input space, and linear kernel. (c) Noninvasive prediction for each observation (continuous) and catheter measurement (dashed). (d) Bland–Altman plot of errors.

TABLE III
VALUES OF R_{ic} FOR EACH SVR ESTIMATING τ, FROM VELOCITY (V) PLUS FEATURES (FV), WITH $d = 4$ (LINEAR KERNEL)

	V lin	FV lin
#1	0.66	0.70
#2	0.78	0.79
#3	0.95	0.96
#4	0.74	0.84
#5	0.75	0.77
#6	0.80	0.80
#7	0.45	0.46
#8	-0.16	-0.16
#9	0.21	0.22
Total	0.58	0.61

CDMM image for estimating τ was found at the very end of the ejection flow velocity field, and the mean standardized regression coefficient was negative at this time instant. Again, this finding in accordance of our previous observations inversely correlating τ to the time and extent of the reverse pressure gradient caused by end-systolic flow deceleration [29].

TABLE IV
MEAN AND 95% CONFIDENCE INTERVALS FOR THE COEFFICIENTS OF CLINICAL VARIABLES IN τ REGRESSION MODEL ($d = 4$)

	τ
HR	22.2 (20.3,24.2)
$(HR)^2$	0.4 (-1.8, 2.8)
LVP	34.6 (28.0,41.2)
$(LVP)^2$	-11.6 (-16.0,-7.3)
EF	-17.1 (-21.3,-13.0)
$(EF)^2$	-14.1 (-17.0,-11.1)

D. Additional Technical Improvement

As far as the linear kernel exhibited a higher acceptable prediction accuracy, we explored the least squares (LS) solution for comparison purposes, but extremely poor performance was obtained for $d = 4$. Hence, for $E_{\max}$ and τ estimations using the least squares solution, we obtained $R_{ic} = 0.16$ and 0.14, respectively. Two possible reasons for the linear SVM outperforming the LS method can be the following. First, the SVM implicitly follows the structural risk minimization principle [20], which leads to better regularization properties than LS in high-dimensional input spaces. And second, from a maximum likelihood

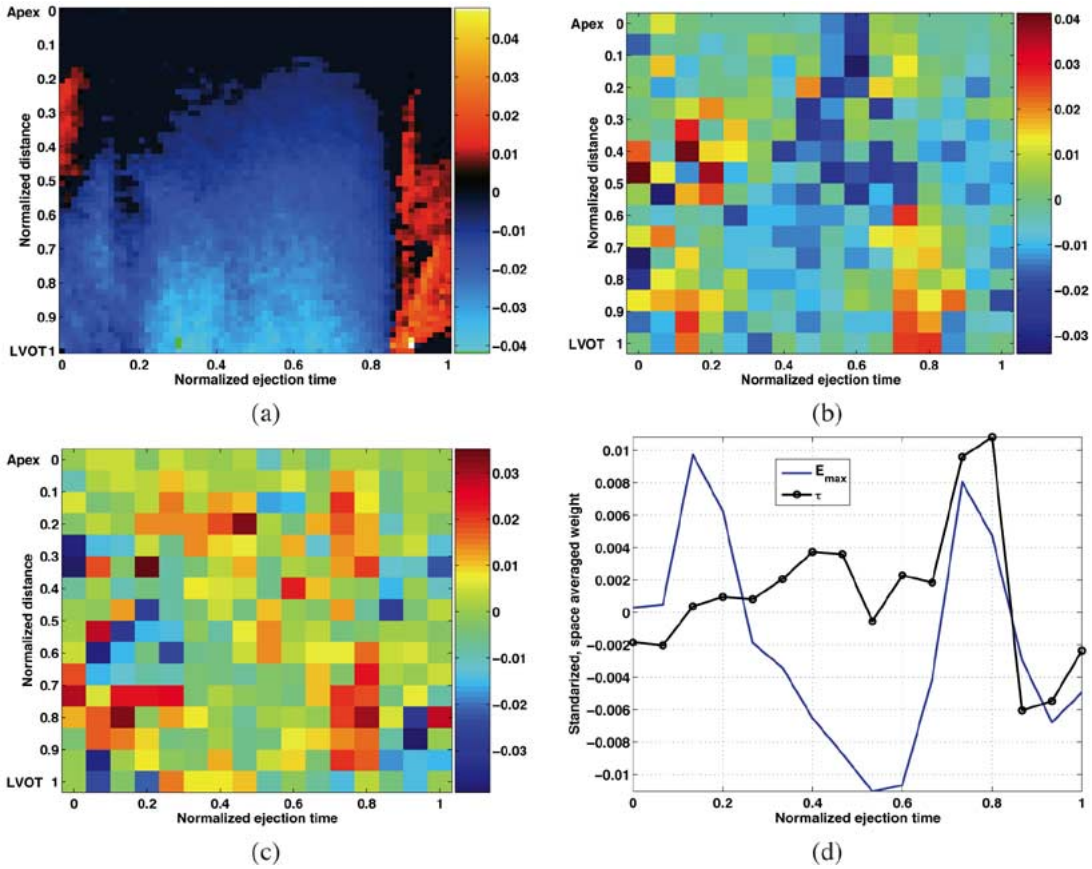

Fig. 2. Linear SVM coefficients representation. (a) Example of centered and normalized Doppler M-mode image. (b) and (c) Map of standardized average coefficients for $E_{\max}$ and τ regression models, respectively. (d) Space-averaged standardized coefficients.

point of view, the LS is appropriate for Gaussian perturbations (which seems not to be the case here), whereas the ε-Huber cost function of the residuals is tuned in the SVM for dealing with different kinds of noise.

In order to determine if an increase in the detail of the CDMM image entered in the input space could improve performance, we repeated the experiments increasing the level of detail. Resolutions corresponding to details $d = 5$ and $d = 6$ were explored, with no significant improvement either in $E_{\max}$ (0.80 for $d = 5$ and 0.79 for $d = 6$) or in τ (0.62 for $d = 5$ and 0.61 for $d = 6$).

IV. Conclusion

An innovative approach has been presented for noninvasively and quantitatively characterizing left ventricular function. Instead of a theoretically-based *a priori* rationale, the possibility of approximating the implicit physical description between a medical image modality and a clinically relevant cardiac index has been proposed with a learning from examples approach. In particular, the use of SVM is illustrated as a potential method to manage full-image input spaces. Furthermore, its SR version has shown to be suitable for extending the input space to decide the convenience of including complementary clinical measurements, thus potentially simplifying medical decision making. Using this methodology, the estimation of two relevant cardiac function indices such as $E_{\max}$ and τ represents a first step in this direction.

Although acceptable for a first approach, the accuracy obtained in the estimation of $E_{\max}$, and particularly of τ, needs to be improved before the method is introduced into clinical practice. A number of SVM processing and data acquisition issues may account for this suboptimal agreement. Regarding the first, the sequential search of the four/five free parameters sometimes became suboptimal, probably explaining why the RBF kernel did not improve the linear kernel. As an exhaustive search is not currently feasible for medium and large scale problems, a better search strategy for free parameters will surely improve the method. Additionally, curse of dimensionality could be present for schemes with increased resolution, an issue that might explain the absence of a significant effect of further image detail on predictive accuracy. Thus, alternative Mercer's kernels, capable of dealing more efficiently with increased detail in the input space, deserve to be explored.

A number of technical aspects of image acquisition may also account for the less than optimal accuracy observed in the present study. Obtaining the true velocity distribution within the LV requires that the Doppler scanline goes through the center of the LV outflow tract as well as the apex. Thus, occasionally anatomical and operator limitations may preclude a fully coaxial interrogation of the ejection flow, which, in turn, translates into underestimated ejection velocities. Although we have demonstrated that significant misalignment is needed to cause a clinically relevant modification in Doppler parameters

[12], this may sometimes limit the applicability of the method in the clinical setting.

We believe this novel approach has potential clinical implications. As previously discussed, we found a number of concordant results of the present study with previous [12], [29], analyses from our group. This suggests that learning from samples methods can be useful when attempting to extract clinical features from novel diagnostic techniques and image modalities. Careful post-hoc analysis of the results of these blind methods may help to find the physiological rationality beyond the searched clinical relationships. Furthermore, learning from samples methods eventually may become a realistic method to extract clinically relevant information directly from medical image modalities. We believe this methodology definitely deserves further exploration in the field of noninvasive cardiovascular diagnosis.

REFERENCES

[1] D. A. Kass, "Assessment of diastolic dysfunction: Invasive modalities," *Cardiol. Clin.*, vol. 18, no. 3, pp. 571–586, 2000.

[2] G. P. Aurigemma and W. H. Gaasch, "Clinical practice: Diastolic heart failure," *New Eng. J. Med.*, vol. 351, no. 11, pp. 1097–1105, 2004.

[3] D. Burkhoff, I. Mirsky, and H. Suga, "Assessment of systolic and diastolic ventricular properties via pressure-volume analysis: a guide for clinical, translational, and basic researchers," *Amer. J. Physiol. Heart Circ. Physiol.*, vol. 289, no. 2, pp. H501–H512, 2005.

[4] M. A. Quinones, "Assessment of diastolic function," *Prog. Cardiovasc. Dis.*, vol. 47, no. 5, pp. 340–355, 2005.

[5] G. P. Aurigemma, M. R. Zile, and W. H. Gaasch, "Lack of relationship between Doppler indices of diastolic function and left ventricular pressure transients in patients with definite diastolic heart failure," *Amer. Heart J.*, vol. 148, no. 3, p. E12, 2004.

[6] M. S. Maurer, D. Spevack, D. Burkhoff, and I. Kronzon, "Diastolic dysfunction: Can it be diagnosed by Doppler echocardiography?," *J. Amer. Coll. Cardiol.*, vol. 44, no. 8, pp. 1543–1549, 2004.

[7] P. Brun, C. Tribouilloy, A. M. Duval, L. Iserin, A. Meguira, G. Pelle, and J. L. Dubois-Rande, "Left ventricular flow propagation during early filling is related to wall relaxation: A color M-mode Doppler analysis," *J. Amer. Coll. Cardiol.*, vol. 20, no. 2, pp. 420–432, 1992.

[8] M. J. Garcia, M. A. Ares, C. Asher, L. Rodriguez, P. Vandervoort, and J. D. Thomas, "An index of early left ventricular filling that combined with pulsed Doppler peak and velocity may estimate capillary wedge pressure," *J. Amer. Coll. Cardiol.*, vol. 29, no. 2, pp. 448–454, 1997.

[9] S. F. Nagueh, N. M. Lakkis, K. Middleton, W. H. Spencer, W. A. Zoghbi, and M. A. Quinones, "Doppler estimation of left ventricular filling pressures in patients with hypertrophic cardiomyopathy," *Circulation*, vol. 99, no. 2, pp. 254–261, 1999.

[10] C. Rivas-Gotz, M. Manolios, V. Thohan, and S. F. Nagueh, "Impact of left ventricular ejection fraction on estimation of left ventricular filling pressures using tissue Doppler and flow propagation velocity," *Amer. J. Cardiol.*, vol. 91, no. 6, pp. 780–784, 2003.

[11] R. Yotti, J. Bermejo, J. C. Antoranz, J. L. Rojo-Álvarez, C. Allue, J. Silva, M. M. Desco, M. Moreno, and M. A. Garcia-Fernandez, "Noninvasive assessment of ejection intraventricular pressure gradients," *J. Amer. Coll. Cardiol.*, vol. 43, no. 9, pp. 1654–1662, 2004.

[12] R. Yotti, J. Bermejo, M. Desco, J. Antoranz, J. L. Rojo-Álvarez, C. Cortina, C. Allue, H. Rodriguez-Abella, M. Moreno, and M. Garcia Fernandez, "Doppler-derived ejection intraventricular pressure gradients provide a reliable assessment of left ventricular systolic chamber function," *Circulation*, vol. 112, pp. 1771–1779, 2005.

[13] J. Thomas and Z. Popovic, "Intraventricular pressure differences: a new window into cardiac function," *Circulation*, vol. 112, pp. 1684–1686, 2005.

[14] Z. Wang, F. Jalali, Y. Sun, J. Wang, K. Parker, and J. Tyberg, "Assessment of left ventricular diastolic suction in dogs using wave-intensity analysis," *Amer. J. Physiol. Heart Circ. Physiol.*, vol. 288, pp. H1641–H1651, 2005.

[15] D.-Y. Tsai, "Comparison of four computer-aided diagnosis schemes for automated discrimination of myocardial heart disease," in *Proc. ICSP2000*, 2000, pp. 2000–2003.

[16] I. Hunter, J. Soraghan, and T. McDonagh, "Fully automatic left ventricular boundary extraction in echocardiographic images," in *Proc. IEEE Comput. Cardiol.*, Sep. 1995, pp. 741–744, "," , pp. 741–744, Sep. 1995.

[17] T. Brotherton, T. Pollard, P. Simpson, and A. DeMaría, "Classifying tissue and structure in echocardiograms," *IEEE Eng. Med. Biol. Mag.*, vol. 13, no. 5, pp. 754–760, Nov./Dec. 1994.

[18] C. Yi, E. Micheli-Tzanakou, D. Shindler, and J. Kostis, "Study of echocardiogram for myocardial infarction using neural networks," in *EMBS Annu. Conf.*, 1993, pp. 255–256.

[19] S. Gazula, A. Hall, and S. Kovács, "Contour extraction of Doppler velocity profiles using neural networks," in *Proc. IEEE Comput. Cardiol.*, Oct. 1992, pp. 543–546.

[20] V. Vapnik, *The Nature of Statistical Learning Theory*. New York: Springer-Verlag, 1995.

[21] M. P. Martínez-Ruíz, M. Gómez-Borja, A. Mollá-Descals, and J. L. Rojo-Álvarez, "La influencia de las características del descuento de precio promocional minorista sobre las ventas: Aplicación de un modelo semiparamétrico," *Rev. Esp. Inv. Market.*, to be published.

[22] J. L. Rojo-Álvarez, M. Martínez-Ramón, A. R. Figueiras-Vidal, M. de-Prado Cumplido, and A. Artés-Rodríguez, "Support vector method for ARMA system identification," *IEEE Trans. Signal Process.*, vol. 52, no. 1, pp. 155–164, Jan. 2004.

[23] J. L. Rojo-Álvarez, A. Figueiras-Vidal, M. Martínez-Ramón, A. García-Armada, and A. Artés-Rodríguez, "A robust support vector algorithm for non-parametric spectral analysis," *IEEE Signal Process. Lett.*, vol. 10, no. 11, pp. 320–323, Nov. 2003.

[24] C. Cortes and V. Vapnik, "Support vector networks," *Mach. Learn.*, vol. 20, pp. 273–297, 1995.

[25] J. L. Rojo-Álvarez, A. Arenal-Maíz, and A. Artés-Rodríguez, "Discriminating between supraventricular and ventricular tachycardias from EGM onset analysis," *IEEE Eng. Med. Biol. Mag.*, vol. 21, no. 1, pp. 16–26, Jan. 2002.

[26] J. L. Weiss, J. W. Frederiksen, and M. L. Weisfeldt, "Hemodynamic determinants of the time-course of fall in canine left ventricular pressure," *J. Clin. Invest.*, vol. 58, no. 3, pp. 751–760, 1976.

[27] A. Kono, W. L. Maughan, K. Sunagawa, K. Hamilton, K. Sagawa, and M. L. Weisfeldt, "The use of left ventricular end-ejection pressure and peak pressure in the estimation of the end-systolic pressure-volume relationship," *Circulation*, vol. 70, no. 6, pp. 1057–1065, 1984.

[28] J. Bermejo, J. C. Antoranz, R. Yotti, M. Moreno, and M. A. Garcia-Fernandez, "Spatio-temporal mapping of intracardiac pressure gradients. A solution to Euler's equation from digital postprocessing of color Doppler M-mode echocardiograms," *Ultrasound Med. Biol.*, vol. 27, no. 5, pp. 621–630, 2001.

[29] R. Yotti, J. Bermejo, C. Antoranz, J. Silva, C. Allue, J. L. Rojo-Álvarez, M. Moreno, and M. Garcia Fernandez, "Noninvasive assessment of ventricular relaxation and contractility indices by analysis of intraventricular ejection pressure-gradient curves derived from Doppler echocardiography," *J. Amer. Coll. Cardiol.*, vol. 41 (Suppl 2), no. 6, p. 447, 2003.